

Theoretical study of the ammonia nitridation rate on an Fe (100) surface: A combined density functional theory and kinetic Monte Carlo study

Sang Chul Yeo,¹ Yu Chieh Lo,² Ju Li,² and Hyuck Mo Lee^{1,a)}

¹Department of Materials Science and Engineering, KAIST, 291 Daehak-ro, Yuseong-gu, Daejeon 305-701, South Korea

²Department of Nuclear Science and Engineering and Department of Materials Science and Engineering, Massachusetts Institute of Technology, Cambridge, Massachusetts 02139, USA

(Received 16 July 2014; accepted 16 September 2014; published online 3 October 2014)

Ammonia (NH₃) nitridation on an Fe surface was studied by combining density functional theory (DFT) and kinetic Monte Carlo (kMC) calculations. A DFT calculation was performed to obtain the energy barriers (E_b) of the relevant elementary processes. The full mechanism of the exact reaction path was divided into five steps (adsorption, dissociation, surface migration, penetration, and diffusion) on an Fe (100) surface pre-covered with nitrogen. The energy barrier (E_b) depended on the N surface coverage. The DFT results were subsequently employed as a database for the kMC simulations. We then evaluated the NH₃ nitridation rate on the N pre-covered Fe surface. To determine the conditions necessary for a rapid NH₃ nitridation rate, the eight reaction events were considered in the kMC simulations: adsorption, desorption, dissociation, reverse dissociation, surface migration, penetration, reverse penetration, and diffusion. This study provides a real-time-scale simulation of NH₃ nitridation influenced by nitrogen surface coverage that allowed us to theoretically determine a nitrogen coverage (0.56 ML) suitable for rapid NH₃ nitridation. In this way, we were able to reveal the coverage dependence of the nitridation reaction using the combined DFT and kMC simulations.

© 2014 AIP Publishing LLC. [<http://dx.doi.org/10.1063/1.4896610>]

I. INTRODUCTION

Ammonia (NH₃) gas nitridation of metals is a commonly used heat treatment for improving surface hardness, mechanical properties, and wear and corrosion resistance as this process incorporates chemically stable nitride compounds to create multi-functional materials for use in various industrial applications.¹⁻⁷ However, NH₃ gas nitridation is a time-consuming process. Various research groups have investigated NH₃ nitridation techniques. Xuan *et al.*⁸ employed both simulations and experiments to develop a self-consistent diffusion model for simulating atomic nitrogen transport in titanium alloys through the coupling effect of both the initial activated nitrogen concentration and a high-temperature gradient. Other groups have reported stable austenitic structures in medical stainless steels that meet the requirements for surgical implantation.⁹ To understand the exact NH₃ nitridation process, a fundamental theoretical study is needed.¹⁰ Specially, the mechanisms for rapid NH₃ nitridation rate have not yet been elucidated. In addition, investigations of catalytic properties on a metal surface must include an examination of the reaction-poisoning or reaction-promoting influence of surface coverage on various reaction mechanisms. The Ertl group reported adsorbate-absorbate interactions based on a statistical analysis of scanning tunneling microscopy results at 300 K.¹¹ Zheng *et al.* measured the coverage-dependent diffusion coefficient for the surface diffusion of hydrogen on a flat Pt (111) surface over a wide coverage range, from 0.1 to 0.8 ML (ML stands for mono-layer),

by linear optical diffraction (LOD).¹² In addition, Nobuhara *et al.* studied the coverage dependence of the H-induced relaxation of a Pd lattice and the corresponding variation in the energy barrier for H adsorption.¹³ The kinetic Monte Carlo (kMC) simulations offer a suitable method for determining rate conditions and have recently been applied by a number of groups to examine the relative rates of competing reactions on surfaces.¹⁴⁻²⁰

We studied NH₃ gas nitridation in real time via kMC simulations. We propose that pre-coverage with nitrogen on an Fe surface may affect the nitridation rate. The reliability of the kMC simulations depends on accurate transition rates, which denote events.²¹⁻²⁵ The effect of surface coverage on an NH₃ nitridation process can be divided into 5 steps: adsorption, desorption, dissociation, penetration of the dissociated nitrogen, and diffusion into the bulk Fe. To simulate all nitridation reaction steps, we quantitatively obtained the adsorption energy, dissociation barrier, penetration energy barrier for the dissociated nitrogen, and surface migration energy barrier of the nitrogen for various surface coverages ($\theta = 0.22$ ML, 0.56 ML, 0.78 ML, 1.00 ML when θ is coverage).²⁶⁻²⁸ This paper is organized as follows. Section II presents the computational methods and systems. Section III provides the density functional theory (DFT) calculation and kMC simulation results. Finally, we discuss our findings in terms of how to improve the nitridation rate using the surface coverage effect and state our conclusions in Sec. IV.

II. COMPUTATIONAL DETAILS

We performed calculations using the Vienna *ab initio* simulation package, a plane-wave code that employs

^{a)} Author to whom correspondence should be addressed. Electronic mail: hmlee@kaist.ac.kr. Tel.: +82-42-350-3334. Fax: +82-42-350-3310.

projector augmented wave method.^{29–32} The spin-polarized DFT calculation was performed with the generalized gradient approximation for the exchange-correlation functional using the PBE method.³³ DFT calculations have previously been shown to aid the mapping of the energetics of various reaction paths. To determine the reaction events, we used a (3×3) super-cell containing a five-layer slab with two fixed layers and a 15-Å vacuum. Only the top 3 layers were allowed to relax. We used an energy cutoff of 400 eV and a $(5 \times 5 \times 1)$ Monkhorst-Pack grid for k-point sampling. We obtained a lattice parameter of 2.83 Å, a bulk modulus of 1.76 Mbar, a cohesive energy of 5.16 eV, and a magnetic moment of $2.21 \mu_B$, which constituted the bulk properties of the pure bcc Fe used for ferromagnetic iron. All values were in good agreement with the literature.³⁴ The adsorption energy (E_{ad}) of the adsorbate, NH_x ($x = 0–3$), for each reaction was calculated according to Eq. (1):

$$E_{ad} = E_{x/surface} - E_{surface} - E_{NH_x}, \quad (1)$$

in which $E_{x/surface}$, E_{NH_x} , and $E_{surface}$ are the total energies of the adsorbed system, the adsorbate, and the clean surface, respectively. A negative adsorption energy corresponds to an energetically favorable adsorption site on the surface. Larger

negative values correspond to stronger adsorption. The energy barrier (E_b) for each reaction was computed according to Eq. (2):

$$E_b = E_{TS} - E_{IS}, \quad (2)$$

in which E_b , E_{TS} , and E_{IS} are the energy barrier of the elementary step, the total energy of the transition state, and the total energy of the initial state, respectively.

The energy (ΔE) for each reaction was computed according to Eq. (3):

$$\Delta E = E_{FS} - E_{IS}, \quad (3)$$

in which E_{TS} , E_{FS} , and E_{IS} are the total energy of transition state, final state, and initial state, respectively. A negative reaction energy indicates that the process is exothermic, whereas a positive value indicates that the process is endothermic. We employed the climbing image nudged elastic band (CI-NEB) method to construct the minimum energy pathway (MEP).³⁵ To examine the effect of surface coverage, we adopted a pre-covered nitrogen atom within a covered Fe (100) (3×3) surface ($\theta = 0.22$ ML, 0.56 ML, 0.78 ML, 1.00 ML), as depicted in Fig. 1.

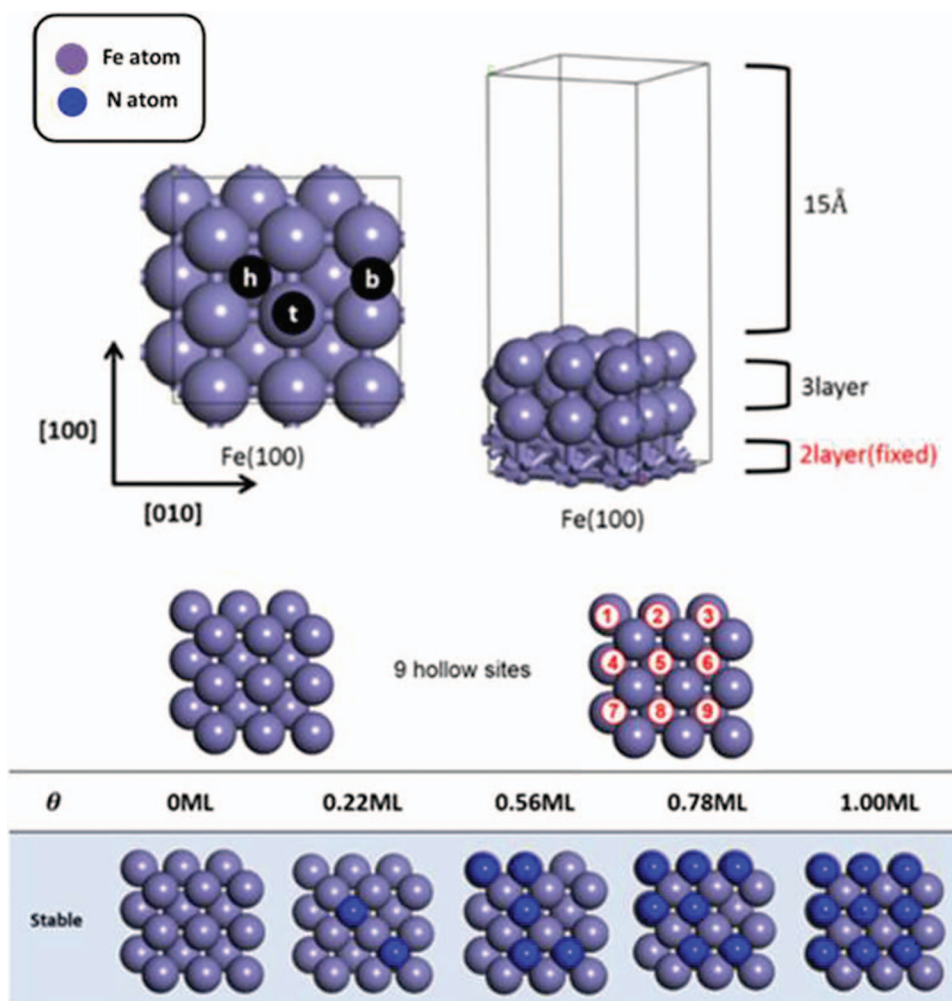


FIG. 1. Structural configuration of a 3×3 super-cell containing five Fe (100) layers. The “h” in the black circle denotes a hollow site, “b” denotes a bridge site, and “t” denotes a top site. The various N pre-covered surfaces were first optimized ($\theta = 0$ ML, 0.22 ML, 0.56 ML, 0.78 ML, and 1.00 ML). The purple and blue spheres represent the Fe and N atoms and a vacuum of 15 Å.

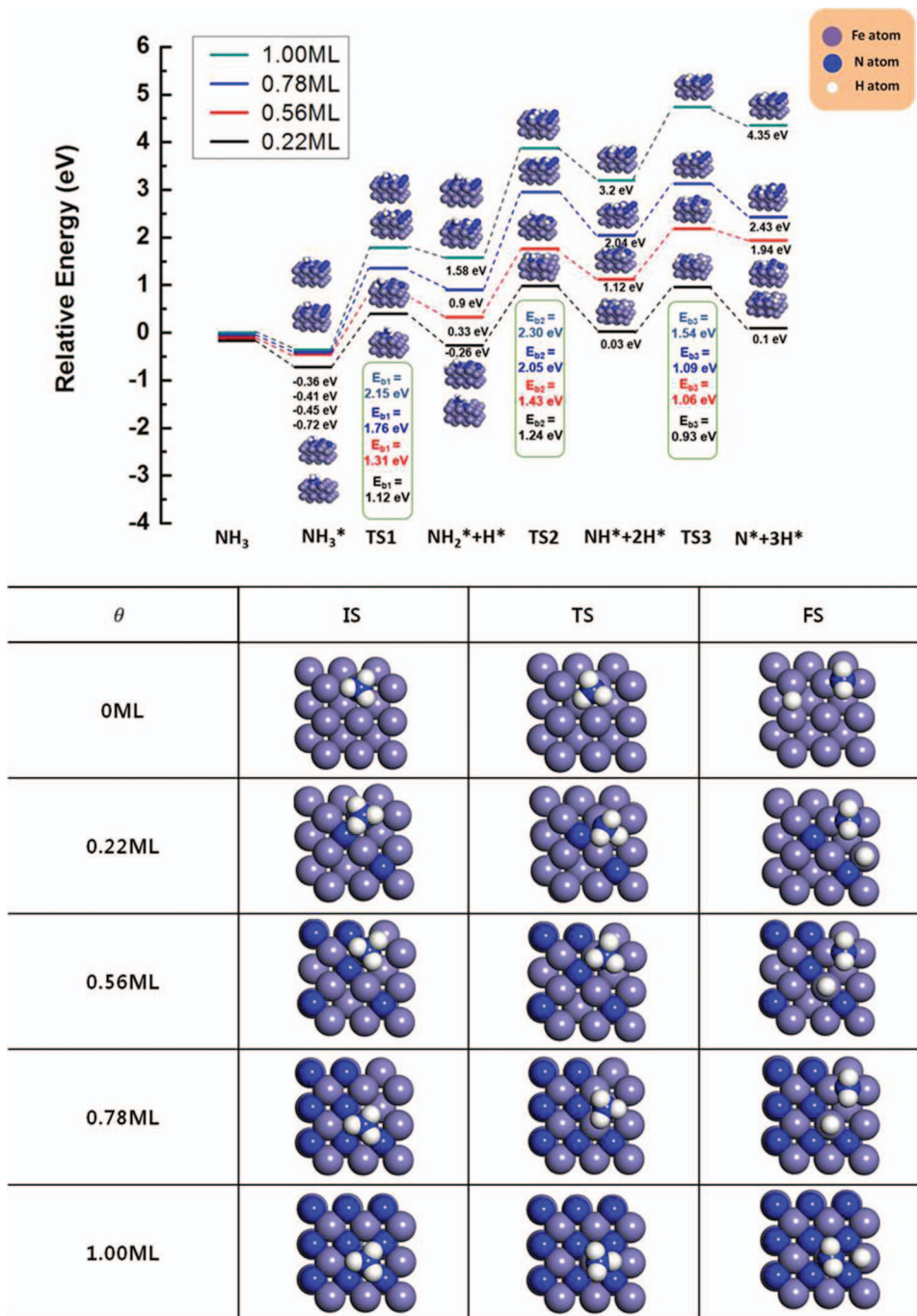


FIG. 2. Reaction pathway and configuration of the initial state (IS), transition state (TS), and final state (FS) for an ammonia-initiated dehydrogenation reaction on various nitrogen pre-covered surfaces ($\theta = 0$ ML, 0.22 ML, 0.56 ML, 0.78 ML, and 1.00 ML).

We employed the kMC algorithm implemented in our C code^{36–38} to investigate the NH_3 nitridation rate on a N pre-covered Fe surface. In a kMC simulation, the temporal evolution of the system is described by a stochastic trajectory. The states along this trajectory are connected by processes associated with the following probabilities: $r_i = v_o e^{-E_i/k_B T}$ in which $v_o = 2k_B T/h$ is on the order of the atomic vibrational frequency and E_i is the energy barrier associated with event i . T is the temperature, k_b is the Boltzmann's constant, and h is the Planck's constant. This form for the rates implies that, in a kMC model, events with a high probability will occur more frequently. At each time step, all rates are calculated

for the given system configuration. In general, the atomic vibrational modes at these points are also used to calculate the pre-factor in the kinetic Monte Carlo. For all events in this study, we used a standard value of 10^{13} s^{-1} for the atomic pre-factor Ω . To select which event will occur at a given time step, a total transition rate R is constructed as follows: $R = \sum_{i=1}^N r_i$ for N possible events in a given system configuration. A uniformly distributed number $\rho_1 \in [0, 1)$ is calculated, and an event j is selected to occur at the given time step. All possible events can be grouped together to reduce the search time for the event. The temporal evolution of the system is based on the assumption that the probability of an event

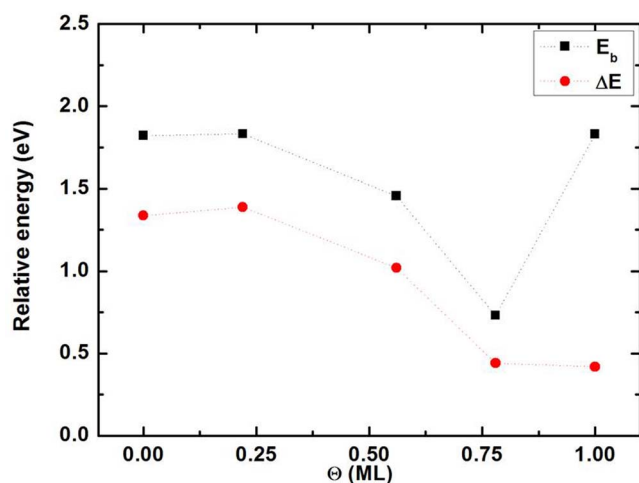


FIG. 3. Energy diagram of both the energy barrier (E_b) and reaction energy (E) for the penetration of dissociated nitrogen at surface coverages of $\theta = 0$ ML, 0.22 ML, 0.56 ML, 0.78 ML, and 1.00 ML. The black line indicates the energy barrier; the red line indicates the reaction energy.

occurring is independent of the system history and therefore obeys Poisson statistics. The probability that an event i occurs in the infinitesimal time interval $(t, t + dt)$ is $p_i(t)dt = r_i dt$, where r_i is the rate associated with that event. The total probability $P(t)$ of an event occurring in the time interval $(t, t + dt)$ is then $P(t)dt = \sum_i p_i(t)dt = \sum_i r_i dt = Rdt$. The probability $p_i(0) = 1$ of no event occurring at time $t = 0$ is unity. The physical time for each time step in the simulation is then assumed to be distributed as in equation: $\sum_{i=1}^{j-1} r_i \leq R\rho_1 < \sum_{i=1}^j r_i$ and a second random number, $\rho_2 \in (0, 1)$, is chosen such that the physical time τ is given by $\rho_2 = e^{-R\tau}$ or $\tau = -\frac{\ln(\rho_2)}{R}$. This expression yields an average time of $1/R$ between events, with the result that simulation time is able to reflect physical time.^{39,40} The Fe (100) surface with a bcc structure forms 40 layers and has a vacuum level of 4 Å. The initial configuration of the NH_3 content (10–90 NH_3 molecules) was confirmed and the temperature was set at 850 K reflecting the experimental condition for NH_3 gas nitridation. The simulation step was set at 10×10^6 steps.

III. RESULTS AND DISCUSSION

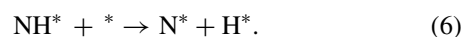
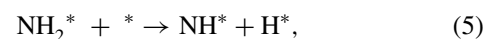
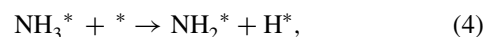
A. DFT calculation of elementary reaction events

In the DFT calculation, we obtained the adsorption energy (E_{ad}) and energy barrier (E_b) for the relevant elemen-

tary processes within the complete NH_3 nitridation mechanism. The reaction was divided into 5 steps (adsorption, dissociation, penetration, surface migration, and diffusion) on an N pre-covered Fe (100) surface. In the first step, adsorption, we investigated the adsorption properties of N and NH_3 on the Fe (100) surface. The results indicated that N adsorbs onto 4-fold hollow sites ($E_{ad} = -1.66$ eV). It was previously reported that NH_3 prefers a top site on the Fe atom for adsorption.⁴¹ The NH_3 adsorbs onto a top site ($E_{ad} = -0.92$ eV) on a clean Fe surface, and the adsorption energy for NH_3 decreases as the surface coverage increases. In this study, energies of -0.72 eV, -0.48 eV, -0.41 eV, and -0.36 eV were obtained at $\theta = 0.22$ ML, 0.56 ML, 0.78 ML, and 1.00 ML, respectively.

Next, we investigated the effect of surface coverage on the dissociation reaction, which is considered the high-energy barrier for full ammonia (NH_3) dehydrogenation. To consider the nitrogen surface coverage effect at each reaction event throughout the process, we employed DFT calculations on a low index (100) of the Fe surface, which is the most stable surface. In addition, the nitrogen-covered Fe (100) surface was modeled using different surface nitrogen concentrations.

Fig. 2 indicates that the reaction pathway for NH_3 dissociation is divided into three elementary steps. In these steps, the corresponding sequence of intermediate steps for NH_3 dissociation can be written as follows:



The * symbols denote an empty site and an adsorbed NH_a ($a = 0-3$) intermediate species on the Fe surface. These dehydrogenation steps are highly reducible. According to Fig. 2, the NH_3 dissociation reactions have a rate-determining step (5). Using the DFT calculations, we obtained the energy barrier (E_b) for the NH_3 dissociation. As the surface coverage increased, the dissociation energy barrier increased. Other research groups have reported that an increase in the surface coverage affects the energy barrier for the dissociation reactions of various species.⁴²⁻⁴⁴ Our results indicated energy barriers of 1.24 eV, 1.43 eV, 2.05 eV, and 2.30 eV at $\theta = 0.22$ ML, 0.56 ML, 0.78 ML, and 1.00 ML, respectively. In our previous study, the energy barrier results for the reaction step (4) were

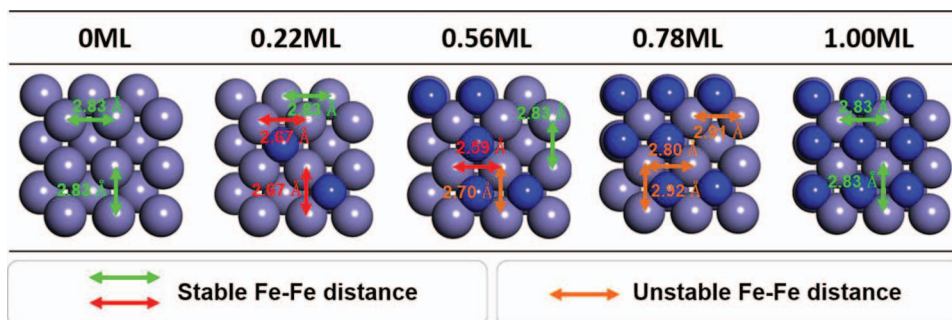


FIG. 4. Surface Fe-Fe distance on various N pre-covered surfaces ($\theta = 0$ ML, 0.22 ML, 0.56 ML, 0.78 ML, and 1.00 ML). The purple and blue spheres represent the Fe and N atoms, respectively. The green and red arrows indicate stable bond lengths, whereas the orange arrows denote unstable bond lengths.

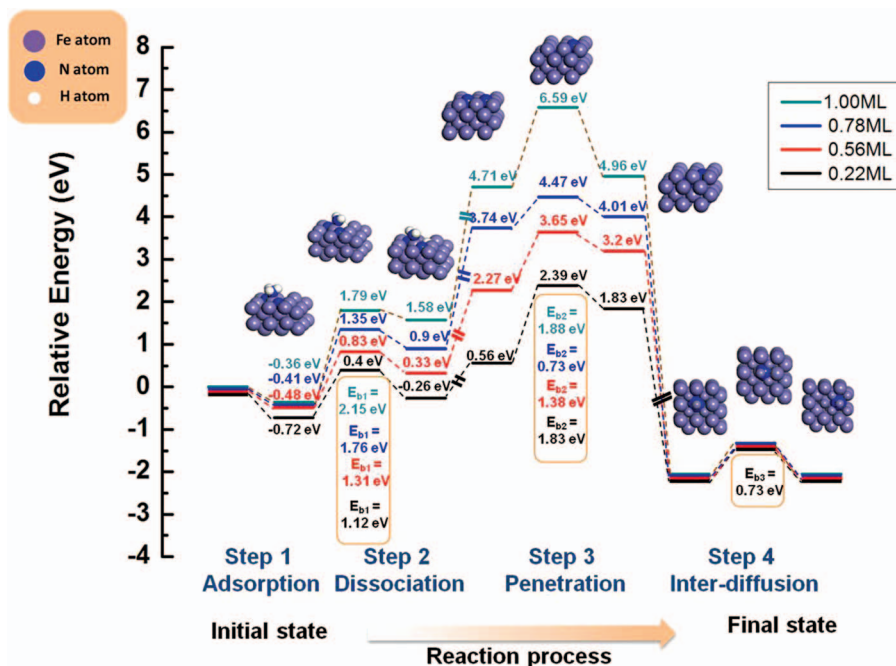


FIG. 5. Reaction pathway of molecular N in N pre-covered bcc-Fe. The black line indicates its behavior at an N coverage of 0.22 ML; the red line indicates its behavior at an N coverage of 0.56 ML; the blue line indicates its behavior at an N coverage of 0.78 ML; and the green line indicates its behavior at an N coverage of 1.00 ML on Fe (100).

used to estimate the catalytic activity of ammonia decomposition on an Fe catalyst.⁴⁵

During the surface migration reaction step, the surface migration energy barrier was considered. Because the dissociated nitrogen atom is expected to migrate from one hollow site to the nearest adjacent hollow site, this surface migration step, which also contributed to the surface coverage effect, should be considered. The results indicated that the surface migration energy barrier was dominant over the surface coverage, with values of 0.9 eV, 0.66 eV, 0.33 eV, and 0.33 eV at $\theta = 0.22$ ML, 0.56 ML, 0.78 ML, and 1.00 ML, respectively.

During the penetration reaction step, a nitrogen atom moves from a hollow site on the surface to an octahedral site

in the sub-layer. We performed DFT calculations to examine the effect of surface coverage on the penetration of the surface-dissociated nitrogen atom into the sub-surface. The results are presented in Fig. 3, in which the energy barriers (E_b) and reaction energies (ΔE) are plotted for the penetration of a dissociated nitrogen at various surface coverages ($\theta = 0$ ML, 0.22 ML, 0.56 ML, 0.78 ML, and 1.00 ML). Jiang and Carter⁴⁶ indicated that a carbon atom diffuses into Fe (100) and Fe (110) with energy barriers of 1.18 and 1.47 eV, respectively. We previously reported that Fe (100) and Fe (110) have the highest energy barrier for nitrogen penetration, in good agreement with the experimental results presented here.⁴⁷ As the surface nitrogen coverage increased on the Fe surface, the penetration energy barrier decreased. We obtained the lowest penetration energy barrier for the dissociated nitrogen ($E_b = 0.73$ eV) with a surface coverage of 0.78 ML. However, at full coverage (1.00 ML), the energy barrier for the penetration of the dissociated nitrogen atom increased ($E_b = 1.82$ eV). Based on the structural analysis, we determined that the low-energy barrier for the penetration of the dissociated nitrogen is governed by the surface stability. As the surface coverage increased, the surface symmetry was broken and distortion increased. For example, the lattice constant is 2.83 Å at the bare surface but, at the coverage of 0.78 ML, it changed to 2.80 Å in one direction while it increased up to 2.92 Å in another direction as seen in Fig. 4. Thus, the surface stability was reduced and nitrogen penetration was easily induced. When the surface is fully covered by nitrogen, the lattice constant changes back to the original value and thus the surface symmetry is restored (see Fig. 4 at the full coverage). The penetration of the dissociated nitrogen is impeded again, which we call the blocking effect. We primarily focused on the surface coverage, which affects the NH_3 nitridation reactions on the Fe surface. For the diffu-

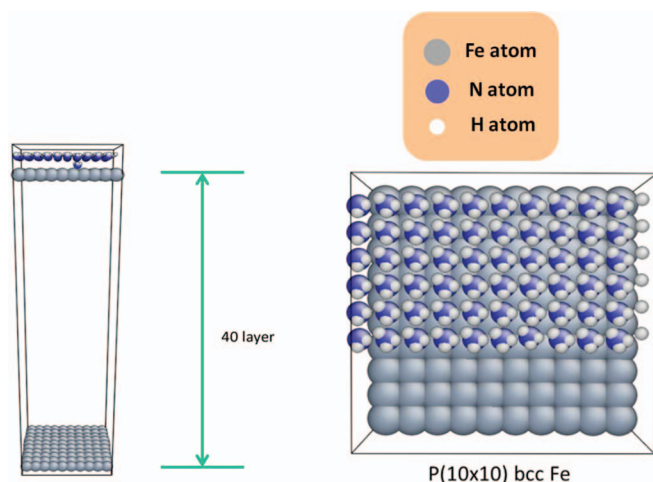


FIG. 6. The initial configuration of the bcc Fe (100) (10×10) with 40 layers and a vacuum level of 4 Å used in the kMC simulation. In this system, the gray, blue, and white spheres represent the Fe, N, and H atom. Non-surface Fe atoms are rendered invisible.

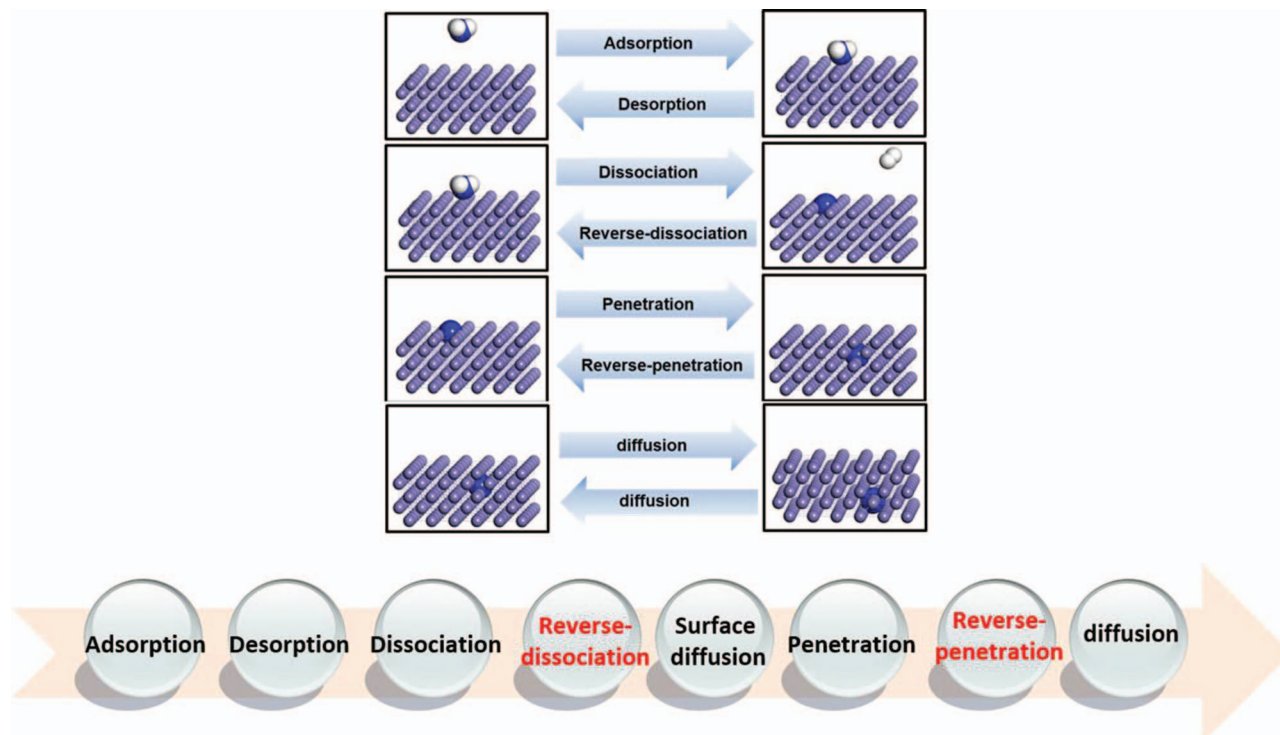


FIG. 7. A list of the NH_3 nitridation reaction events (8 steps). In the upper figure, the purple, blue, and white spheres represent the Fe, N, and H atoms, respectively.

sion reaction step, we constructed an energy diagram for the diffusion of nitrogen into bulk Fe, a process that is generally well characterized. Nitrogen is typically located in the octahedral interstitial sites. Given the energy barrier for nitrogen confirmed in pure bcc-Fe, our result ($E_b = 0.73$ eV) is in good agreement with the experimental results.^{48,49}

We primarily focused on the effect of surface coverage on NH_3 nitridation on the Fe surface. The reaction was divided into adsorption, dissociation, surface migration, penetration, and diffusion. For a quantitative analysis of the surface coverage effect, we reinvestigated NH_3 nitridation as a function of surface coverage. A schematic diagram for the full NH_3 ni-

tridation mechanism is provided in Fig. 5. We described five steps along the reaction pathway.

B. kMC simulations of ammonia nitridation

We performed kMC simulations to confirm the surface coverage effects on the complete process: adsorption, desorption, dissociation, reverse-dissociation, surface migration, penetration, reverse-penetration, and diffusion reactions as determined from the DFT calculations. For the kMC simulation, we utilized a system model for the initial configuration as depicted in Fig. 6. Fig. 7 provides a possible process for the different reactions that occur during NH_3 nitridation, includ-

TABLE I. A list of the nitridation reaction events, consisting of the adsorption energy, activation energy, and pre-factor for each reaction step. The pre-factor denotes the default value.

Event	Elementary reaction	Energy barrier (E_b)	
Adsorption	$\text{NH}_3 + * \rightarrow \text{NH}_3^*$	0 eV	
Desorption	$\text{NH}_3^* \rightarrow \text{NH}_3 + *$	0.22 ML: 0.72 eV	0.56 ML: 0.48 eV
		0.78 ML: 0.41 eV	1.0 ML: 0.36 eV
Dissociation	$\text{NH}_3^* \rightarrow \text{N}^* + 3\text{H}^*$	0.22 ML: 1.24 eV	0.56 ML: 1.43 eV
		0.78 ML: 2.05 eV	1.0 ML: 2.3 eV
Reverse dissociation	$\text{N}^* + 3\text{H}^* \rightarrow \text{NH}_3^*$	0.22 ML: 1.28 eV	0.56 ML: 1.12 eV
		0.78 ML: 0.84 eV	1.0 ML: 0.25 eV
Surface migration	$\text{N}(\text{hollow}) \rightarrow \text{N}(\text{hollow})$	0.22 ML: 0.9 eV	0.56 ML: 0.66 eV
		0.78 ML: 0.33 eV	1.0 ML: 1.00 eV
Penetration	$\text{N}(\text{hollow}) \rightarrow \text{N}(\text{o-site})$	0.22 ML: 1.83 eV	0.56 ML: 1.45 eV
		0.78 ML: 0.73 eV	1.0 ML: 1.83 eV
Reverse penetration	$\text{N}(\text{o-site}) \rightarrow \text{N}(\text{hollow})$	0.22 ML: 0.5 eV	0.56 ML: 0.45 eV
		0.78 ML: 0.4 eV	1.0 ML: 1.6 eV
Diffusion	$\text{N}(\text{o-site}) \rightarrow \text{N}(\text{o-site})$	0.73 eV	

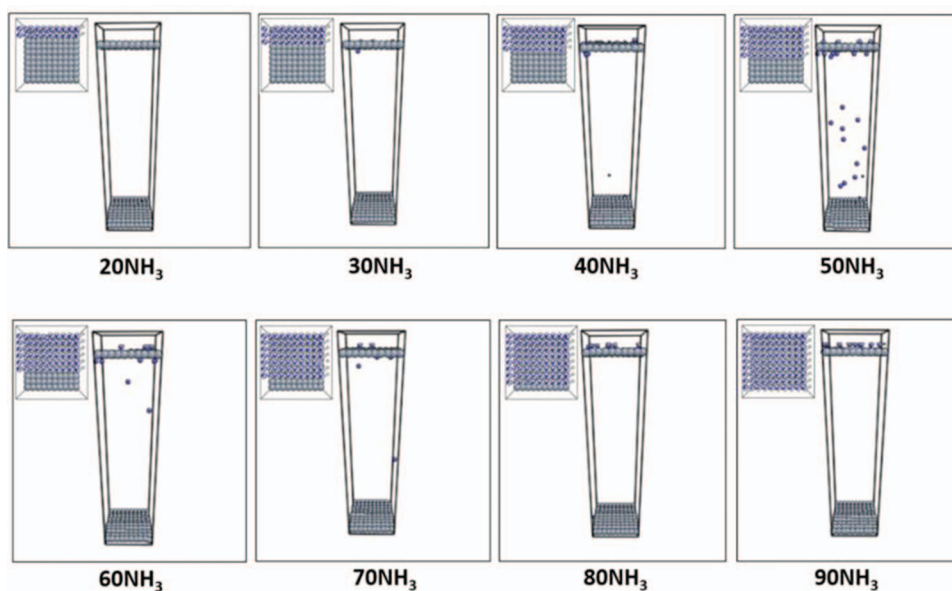


FIG. 8. The NH_3 nitridation results from the kMC simulation. These figures indicate the degree of nitrogen diffusion in bulk bcc Fe at 5×10^6 step of kMC simulation. Initial conditions were decided by NH_3 contents (20, 30, 40, 50, 60, 70, 80, and 90 NH_3) on the vacuum level. Non-surface Fe atoms are rendered invisible for better visualization.

ing a complete list of the NH_3 nitridation reaction events. The first adsorption event has no notable energy barrier. Therefore, we set this event at 0 eV regardless of nitrogen surface coverage. By contrast, the desorption events provided alternatives to the adsorption energy (E_{ad}) set at 0.92 eV, 0.82 eV, 0.72 eV, and 0.62 eV at $\theta = 0.22$ ML, 0.56 ML, 0.78 ML, and 1.00 ML, respectively. Next, using the dissociation reaction event, we obtained energy barriers for the NH_3 dissociation of 1.24 eV, 1.43 eV, 2.05 eV, and 2.30 eV at $\theta = 0.22$ ML, 0.56 ML, 0.78 ML, and 1.00 ML, which are the energy barriers of the rate-limiting step in the full dehydrogenation reaction pathway for NH_3 dissociation. For simplification of calculations, we only considered the rate-limiting step which exclusively determines reaction rate among specified reactions. After dissociation of the NH_3 , the dissociated nitrogen was classified by both its surface migration and penetration from the surface to the sub-layer of the Fe surface. In the case of reactions such as $\text{H} + \text{H} \rightarrow \text{H}_2$ and $\text{N} + \text{N} \rightarrow \text{N}_2$, we did not take into consideration of desorption of H_2 or N_2 gas, which is not concerned with nitridation rate. During the surface migration, energy barriers of 0.9 eV, 0.66 eV, 0.33 eV, and 0.33 eV were determined at $\theta = 0.22$ ML, 0.56 ML, 0.78 ML, and 1.00 ML, respectively. In this study, the penetration reaction occurred at 1.83 eV, 1.45 eV, 0.73 eV, and 1.83 eV at $\theta = 0.22$ ML, 0.56 ML, 0.78 ML, and 1.00 ML, respectively. Finally, the diffusion events were set at 0.73 eV, the energy barrier for nitrogen diffusion in bulk Fe. Because the diffusion events have no effect on N surface coverage on Fe surface.

To obtain an accurate kMC simulation, the reverse reactions must be considered. We considered two reaction events, the reverse reactions of both the dissociation and penetration steps. These reverse dissociation events were determined as 1.28 eV, 1.12 eV, 0.84 eV, and 0.25 eV at $\theta = 0.22$ ML, 0.56 ML, 0.78 ML, and 1.00 ML. These values were obtained using the previous NH_3 dissociation results and are also the en-

ergy barriers for the rate-limiting step in the complete dehydrogenation reaction pathway for NH_3 dissociation, including the reverse reactions. The reverse penetration events were determined by 0.5 eV, 0.45 eV, 0.4 eV, and 1.6 eV at $\theta = 0.22$ ML, 0.56 ML, 0.78 ML, and 1.00 ML, respectively. Table I lists the energy barriers for the 8 possible reaction events.

These results describe the behavior of the NH_3 nitridation reaction using a kMC simulation. We conclude that the nitrogen surface coverage affects the nitridation rate. In order to verify the degree of nitrogen diffusion in the bulk bcc Fe at 5×10^6 step of kMC simulation. In Fig. 8, the initial conditions were decided by the NH_3 contents. We provided simulation snapshots of the nitridation process involving ammonia based on the nitrogen surface coverage ($\theta = 0.22$ ML, 0.56 ML, 0.78 ML, and 1.00 ML). As shown in Fig. 9, we could

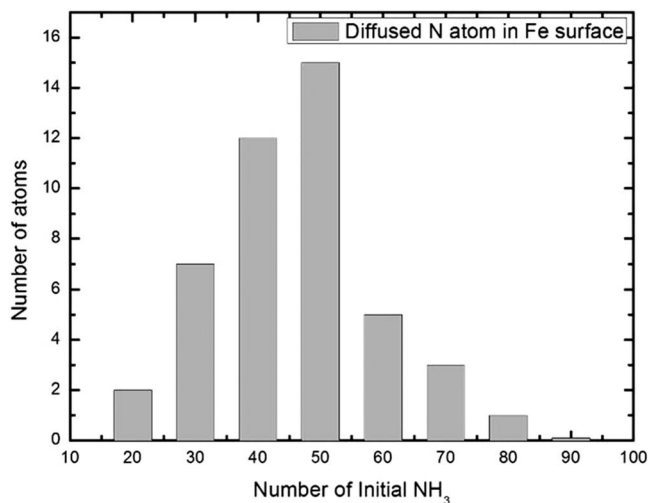


FIG. 9. The results for the number of diffused nitrogen atoms in bcc Fe after full simulation steps at 10×10^6 steps.

easily determine that the number of diffused nitrogen atoms is maximized under the initial condition of 50 NH₃ out of 90 sites on the Fe surface. Considering that the real-time atomistic kMC simulations are based on a database of energy barriers (E_b) obtained from the DFT results, we believe that an increase in the NH₃ nitridation rate can be attained by a nitrogen surface coverage of about 0.56 ML on an N pre-covered Fe surface. It is most likely because distortion of surface is optimum at this value of coverage and the blocking effect becomes dominant at a higher coverage.

IV. CONCLUSION

We studied NH₃ gas nitridation using a combination of DFT and kMC simulations to examine the effect of nitrogen surface coverage on an Fe surface. This research provides a new theoretical approach to estimate the nitridation rate. The mechanism used for the DFT calculation was divided into the adsorption, dissociation, surface migration, and penetration properties (i.e., configuration, site preference, and relative stability) and the diffusion. To investigate the effect of nitrogen surface coverage on each reaction step, we modeled a nitrogen-covered Fe (100) surface with various surface nitrogen concentrations ($\theta = 0.22$ ML, 0.56 ML, 0.78 ML, and 1.00 ML). We then calculated the elementary reaction steps following the mechanism. The reactivity of both the adsorption and dissociation steps decreased as the nitrogen surface coverage increased on the Fe (100) surface. We also examined the surface migration and penetration energy barriers. The surface stability was correlated with the surface symmetry along a surface containing an N pre-covered Fe surface. The nitrogen diffusion was calculated in bulk bcc Fe and found to be in good agreement with the experiment.

Using a database of the DFT calculations, we performed a real-time atomistic simulation using kMC simulations supported by a database of energy barriers (E_b) from the DFT results. The reliability of the kMC simulations depends on accurate transition rates, for events. We concluded that the nitridation rate could be improved by the suitable nitrogen coverage (0.56 ML) on the Fe (100) surface.

ACKNOWLEDGMENTS

This research was supported by a grant from the National Research Foundation of Korea (NRF) funded by the Korean government (MEST) (2011-0028612).

¹T. Weber *et al.*, *Mater. Sci. Eng., A* **199**, 205 (1995).

²D. K. Inia *et al.*, *Appl. Phys. Lett.* **70**, 1245 (1997).

³S. A. Gerasimov *et al.*, *Met. Sci. Heat Treat.* **43**, 462 (2001).

⁴X. Luo and S. X. Liu, *J. Magn. Magn. Mater.* **308**, L1 (2007).

⁵L. Nosei *et al.*, *Thin Solid Films* **516**, 1044 (2008).

⁶W. P. Tong *et al.*, *Science* **299**, 686 (2003).

⁷M. Wohlschlogel, U. Welzel, and E. J. Mittemeijer, *Thin Solid Films* **520**, 287 (2011).

⁸F. Z. Xuan *et al.*, *Comput. Mater. Sci.* **49**, 104 (2010).

⁹P. Wan *et al.*, *J. Mater. Sci. Technol.* **27**, 1139 (2011).

¹⁰M. Rida and H. Tout, *Rev. Metall.-Cah. Inf. Tech.* **107**, 117 (2010).

¹¹G. Ertl and M. Huber, *J. Catal.* **61**, 537 (1980).

¹²C. Z. Zheng *et al.*, *Phys. Rev. B* **70**, 205402 (2004).

¹³K. Nobuhara *et al.*, *J. Appl. Phys.* **92**, 5704 (2002).

¹⁴Y. M. Choi and P. Liu, *Catal. Today* **165**, 64 (2011).

¹⁵A. P. van Bavel *et al.*, *Phys. Chem. Chem. Phys.* **6**, 1830 (2004).

¹⁶M. A. Albao *et al.*, *Surf. Sci.* **617**, 73 (2013).

¹⁷M. Lakhal *et al.*, *Int. J. Hydrogen Energy* **38**, 8350 (2013).

¹⁸S. Lin *et al.*, *J. Phys. Chem. C* **117**, 451 (2013).

¹⁹S. Scarle and C. P. Ewels, *Eur. Phys. J. B* **51**, 195 (2006).

²⁰S. Hong *et al.*, *J. Catal.* **276**, 371 (2010).

²¹A. F. Voter, F. Montalenti, and T. C. Germann, *Annu. Rev. Mater. Res.* **32**, 321 (2002).

²²M. A. Snyder and D. G. Vlachos, *Journal of Chemical Physics* **123**, 184707 (2005).

²³H. X. Xu, Y. N. Osetsky, and R. E. Stoller, *J. Nucl. Mater.* **423**, 102 (2012).

²⁴H. X. Xu, Y. N. Osetsky, and R. E. Stoller, *J. Phys. Condens. Matter* **24**, 375402 (2012).

²⁵B. Hanson, V. Pryamitsyn, and V. Ganesan, *J. Phys. Chem. B* **116**, 95 (2012).

²⁶N. Lopez, M. Garcia-Mota, and J. Gomez-Diaz, *J. Phys. Chem. C* **112**, 247 (2008).

²⁷K. Mudiyansele, M. Trenary, and R. J. Meyer, *J. Phys. Chem. C* **111**, 7127 (2007).

²⁸Z. Rosenzweig, I. Farbman, and M. Asscher, *Journal of Chemical Physics* **98**, 8277 (1993).

²⁹G. Kresse and D. Joubert, *Phys. Rev. B* **59**, 1758 (1999).

³⁰G. Kresse and J. Furthmüller, *Phys. Rev. B* **54**, 11169 (1996).

³¹P. E. Blochl, *Phys. Rev. B* **50**, 17953 (1994).

³²G. Kresse and J. Hafner, *Phys. Rev. B* **48**, 13115 (1993).

³³J. P. Perdew, K. Burke, and M. Ernzerhof, *Phys. Rev. Lett.* **77**, 3865 (1996).

³⁴D. E. Jiang and E. A. Carter, *Phys. Rev. B* **67**, 214103 (2003).

³⁵G. Henkelman, B. P. Uberuaga, and H. Jonsson, *Journal of Chemical Physics* **113**, 9901 (2000).

³⁶J. S. Reese, S. Raimondeau, and D. G. Vlachos, *J. Comput. Phys.* **173**, 302 (2001).

³⁷S. Raimondeau *et al.*, *Ind. Eng. Chem. Res.* **42**, 1174 (2003).

³⁸C. Domain, C. S. Becquart, and L. Malerba, *J. Nucl. Mater.* **335**, 121 (2004).

³⁹A. B. Bortz, M. H. Kalos, and J. L. Lebowitz, *J. Comput. Phys.* **17**, 10 (1975).

⁴⁰K. A. Fichthorn and W. H. Weinberg, *Journal of Chemical Physics* **95**, 1090 (1991).

⁴¹X. Z. Duan *et al.*, *J. Mol. Catal. A: Chem.* **357**, 81 (2012).

⁴²B. Hammer, *Phys. Rev. B* **63**, 205423 (2001).

⁴³E. van Steen and P. van Helden, *J. Phys. Chem. C* **114**, 5932 (2010).

⁴⁴C. Wu *et al.*, *J. Catal.* **286**, 88 (2012).

⁴⁵S. C. Yeo, S. S. Han, and H. M. Lee, *J. Phys. Chem. C* **118**, 5309 (2014).

⁴⁶D. E. Jiang and E. A. Carter, *Phys. Rev. B* **71**, 045402 (2005).

⁴⁷S. C. Yeo, S. S. Han, and H. M. Lee, *Phys. Chem. Chem. Phys.* **15**, 5186 (2013).

⁴⁸Y. Iijima, *J. Alloys Compd.* **234**, 290 (1996).

⁴⁹J. R. G. da Silva and R. B. McLellan, *Mater. Sci. Eng.* **26**, 83 (1976).